Dual-Output Microwave Photonic Frequency Up- and Down-Converter Using a 90° Optical Hybrid Without Filtering

Peiran Jia and Jianxin Ma, *Member, IEEE*

***Abstract*—A dual-output microwave photonic frequency up- and down-converter using a 90° optical hybrid without filtering is proposed. By using a dual-parallel Mach-Zehnder modulator and a Mach-Zehnder modulator in parallel to realize carrier suppressed single sideband and carrier suppressed double sideband modulation, respectively, with a 90° optical hybrid and 90° electrical hybrid coupler, this scheme can implement two functions: simultaneous up- and down-conversion signal generation, or high image rejection in down-conversion. Simulation results show that the proposed structure can achieve an up-conversion with a tunable range of 17–23 GHz or a down-conversion with a tunable range of 1–7 GHz, respectively, based on a fixed 8 GHz LO signal. The unwanted signal suppression ratio of desired signal is about 27.2 dB for up-conversion and 30.0 dB for down-conversion. In addition, we have tested and analyzed the conversion gain, noise figure and spurs free dynamic range of the system. For image rejection in down-conversion, we can achieve an image rejection ratio (IRR) about 65.2 dB. Moreover, the impact of the phase drift, RF frequency, amplitude and phase variation on IRR is discussed. Finally, the influence of half-voltage imbalance of the DPMZM sub-modulators on IRR is analyzed, and a compensation method is given.**

***Index Terms*—Frequency conversion, image reject mixer, microwave photonics, optical hybrid, optical signal processing.**

I. Introduction

MICROWAVE frequency conversion is an important function in wireless communication, satellite repeater, radar systems, and electronic warfare [1]. It either up converts a low-frequency intermediate frequency (IF) signal into a high-frequency radio frequency (RF) one or down converts a high-frequency RF signal into a low-frequency IF one [2]. With the rapid development of communication technology, the converters with higher conversion gain, larger dynamic range and more effective mixing spurs suppression are desired, and so the performance of traditional electrical converters faces great challenges. In recent years, microwave frequency conversion technology has received widespread attention. Compared with traditional electronic frequency conversion method, a microwave photonic converter shows all kinds of advantages including large bandwidth, high isolation, and anti-electromagnetic interference [3]. Numerous microwave photonic conversion methods based on different physical mechanisms have been reported recently. Microwave photonic frequency conversion based on stimulated Brillouin scattering (SBS) effect [4]–[5] was achieved, but the Brillouin frequency shift is usually in the range from 10 to 11 GHz for the silicon medium, which makes it difficult to achieve a wide range of flexible adjustment of the local oscillator (LO) signal. Another problem is that the Brillouin frequency shift drifts is sensitive to temperature and strain, leading to instability of the LO signal frequency. Another method is based on an integrated electro-optic modulator or polarization modulator to realize frequency up- or down-conversion [6]–[9]. In [6], a dual-drive Mach-Zehnder modulator (DDMZM) is used to realize down-conversion without any filter showing a good flexibility and frequency stability. In [7], a dual-parallel Mach-Zehnder modulator (DPMZM) is used to implement the frequency up-conversion with the LO signal frequency doubled, which reduces the bandwidth requirements of both the LO and the optical modulator. In [8], a dual-polarization dual-drive Mach-Zehnder modulator (DPol-DDMZM) is used to generate two quadrature modulated signals, realizing both frequency down-conversion and phase shift functions. In [9], an I/Q down-converter is proposed by using a polarization division multiplexing dual-parallel Mach-Zehnder modulator (PDM-DPMZM) and can realize fundamental or sub-harmonic I/Q down-conversion. In reality, microwave photonic converter is usually implemented through a heterodyne structure to obtain a nonzero IF signal, which is susceptible to be interfered by image signals in down-conversion. Moreover, due to the structure with a single-ended mixer in [6]–[7], it is hardly to suppress the image signal. In order to effectively suppress the image interference, image-reject mixer (IRM) is required. IRM is a down-converter that can suppress largely the undesired image signal at f_{IM} coming from the down converted products ($f_{IMC} = |f_{LO} - f_{IM}|$) while maintaining or even enhancing the wanted component [10]. Recently, phase-cancellation technique is regarded as a good way to realize microwave photonic IRMs, where uses a 90° optical hybrid to achieve the image rejection [11]–[15].

The microwave photonic converters with multiple functions (reconfigurable, image rejection in down-conversion, dual-

Manuscript received April 11, 2022; revised May 23, 2022; accepted June 1, 2022. Date of publication June 7, 2022; date of current version June 14, 2022. This work was supported in part by the National Natural Science Foundation of China under Grant 61690195 and in part by the Fund of State Key Laboratory of IPOC under Grant IPOC2018ZT09. *(Corresponding author: Jianxin Ma.)*

The authors are with the State Key Laboratory of Information Photonics and Optical Communications, and Beijing Key Laboratory of Space-Ground Interconnection and Convergence, School of Electronic Engineering, Beijing University of Posts and Telecommunications, Beijing 100876, China (e-mail: jiapr@bupt.edu.cn; majianxinxy@163.com).

Digital Object Identifier 10.1109/JPHOT.2022.3181031

band/multi-band frequency conversion, up and down frequency conversion switchable) are more preferred [16]–[18]. In [16], a photonics-based four-band RF simultaneous generation scheme is proposed with four 90° optical hybrids and an optical filter, while it has complicated structure and the flexibility of the system is also limited. In [17], a switchable photonic microwave single sideband frequency converter without filtering based on DP-DDMZM is proposed, and frequency conversion can be switched between two different frequency bands by adjusting one DC bias voltage of the sub-DMZM. However, this scheme cannot effectively suppress the image signal because of the single-ended mixer. Moreover, the DC bias voltages should be controlled accurately. In [18], a microwave photonic up-converter with acousto-optic modulator (AOM) is proposed. However, the system bandwidth is limited because the AOM has only a 70 MHz RF bandwidth and a 200 MHz RF working center frequency.

In this paper, we propose and demonstrate a dual-output microwave photonic frequency up- and down-converter based on the phase cancellation technique. This scheme can implement two functions: simultaneous up- and down-conversion signal generation, or high image rejection in down-conversion. Due to the use of carrier suppressed single sideband (CS-SSB) modulation, the mixing spurs are well suppressed without using any optical or electrical filter. Simulation results show that up and down converted signals can be generated simultaneously and output separately through a 90° optical hybrid and a 90° electrical hybrid coupler. The proposed structure can achieve an up-conversion with a tunable range of 17–23 GHz or a down-conversion with a tunable range of 1–7 GHz, respectively, based on a fixed 8 GHz LO signal. The mixing spurs suppression ratio is better than 27 dB. The conversion gain, noise figure and spurs free dynamic range of the system have been tested and analyzed. For image rejection in down-conversion, the image rejection ratio (IRR) can reach 65.2 dB. Moreover, the impact of the phase drift, RF frequency, amplitude and phase variation on IRR is discussed. Finally, the influence of half-voltage imbalance of the DPMZM sub-modulators on IRR is analyzed, and a compensation method is given.

The paper is organized as: In Section II, the working principle of the proposed scheme is introduced, and the principle of image signal suppression in down-conversion is deduced; In Section III, the simulation analysis of the proposed scheme is carried out, and the optical spectra and electrical spectra are presented. Tunability, conversion gain, noise figure and spurs free dynamic range of the system are analyzed. In addition, we analyze the image rejection function and its stability; In Section IV, we compare this scheme with other schemes and analyze the advantages of this scheme. At last, conclusions are drawn in Section V.

II. Principle

A. Simultaneous Up- and Down-Conversion Signal Generation

The schematic diagram of the proposed scheme is shown in Fig. 1. When the signal power input to the optical modulator is small, the power of the high-order sidebands (≥ 2) generated by the optical modulator are at least 20 dB lower than the power of the first-order sideband, so the impact of the high-order sidebands on the system performance can be ignored. Only the first-order sideband spectrum is given in Fig. 1.

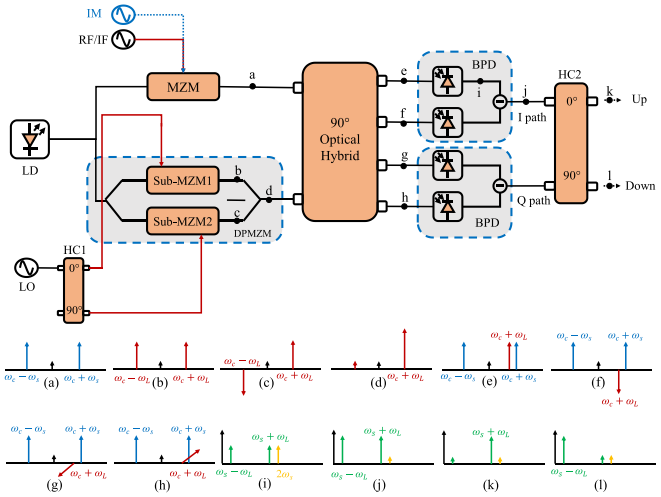

Fig. 1. Schematic diagram of the proposed dual-output microwave photonic frequency up- and down-converter without filtering. LD, laser diode; DPMZM, dual-parallel Mach-Zehnder modulator; MZM, Mach-Zehnder modulator; HC, 90° electrical hybrid coupler; BPD, balanced photodetector. (a–l): The spectrum evolution of optical and electrical signals.

The optical carrier emitted from the CW laser diode (LD), expressed as $E_{in}(t) = E_0 e^{j\omega c t}$ with an amplitude of E_0 and an angular frequency of ω_c, is split into two beams by an optical coupler (OC) and then fed to two electrooptical modulators (MZM and DPMZM). The MZM, biased at the minimum transmission point, is driven by input signal (RF/IF) to realize CS-DSB modulation. The DPMZM, consisting of two sub-MZMs (Sub-MZM1 and Sub-MZM2) embedded in a main-MZM, is driven by the LO signal via its two electrodes with a 90° electrical hybrid coupler (HC1) to realize the CS-SSB modulation. Since the main MZM is operated at the quadrature point while the two sub-MZMs, with equal half-voltage, both work at the minimum transmission points, the modulated optical signal output from MZM and DPMZM can be expressed as,

$$E_{MZM} = \frac{\sqrt{2}}{4} j E_{in}(t) \left[e^{-j\beta_1 \cos(\omega_s t)} - e^{j\beta_1 \cos(\omega_s t)} \right] \approx \frac{\sqrt{2}}{2} E_0 J_1(\beta_1) \left[e^{j(\omega_c+\omega_s)t} + e^{j(\omega_c-\omega_s)t} \right] \quad (1)$$

$$E_{DPMZM} = \frac{\sqrt{2}}{2} \left\{ \begin{array}{l} \frac{1}{4} j E_{in}(t) \left[e^{-j\beta_2 \cos(\omega_L t)} - e^{j\beta_2 \cos(\omega_L t)} \right] \\ -\frac{1}{4} E_{in}(t) \left[e^{-j\beta_2 \sin(\omega_L t)} - e^{j\beta_2 \sin(\omega_L t)} \right] \end{array} \right\} \approx \frac{\sqrt{2}}{2} E_0 J_1(\beta_2) e^{j(\omega_c+\omega_L)t} \quad (2)$$

where ω_s and ω_L are the angular frequencies of the RF/IF signal and LO signal, respectively. V_s and V_L are the amplitude of the RF/IF signal and the LO signal, respectively; the modulation indexes are $\beta_1 = \pi V_s / V_\pi$ for the upper MZM and $\beta_2 = \pi V_L / V_\pi$

for the two sub-MZM; V_π represents the half-voltage of the modulator. $J_n(.)$ is the nth-order Bessel function of the first kind. In (1) and (2), the Jacobi–Anger expansion is used, and the sidebands with the order higher than 2nd are neglected under small signal modulation. The lightwaves output from the MZM and the DPMZM are injected into a 90° optical hybrid, which has two imports and four outports with the 4×2 transmission matrix.

The 90° optical hybrid outputs two in-phase optical signals (E_{Ix}, E_{Iy}) and two orthogonal optical signals (E_{Qx}, E_{Qy}) as follows:

$$T = \begin{bmatrix} 1 & 1 \\ 1 & -1 \\ 1 & j \\ 1 & -j \end{bmatrix} \tag{3}$$

$$\begin{bmatrix} E_{I_x} \\ E_{I_y} \\ E_{Q_x} \\ E_{Q_y} \end{bmatrix} \propto \begin{bmatrix} 1 & 1 \\ 1 & -1 \\ 1 & j \\ 1 & -j \end{bmatrix} \begin{bmatrix} E_{MZM} \\ E_{DPMZM} \end{bmatrix}$$

$$\begin{aligned} E_{I_x} &\propto J_1(\beta_1)\left[e^{j(\omega_c+\omega_s)t} + e^{j(\omega_c-\omega_s)t}\right] \\ &\quad + J_1(\beta_2)\, e^{j(\omega_c+\omega_L)t} \\ E_{I_y} &\propto J_1(\beta_1)\left[e^{j(\omega_c+\omega_s)t} + e^{j(\omega_c-\omega_s)t}\right] \\ &\quad - J_1(\beta_2)\, e^{j(\omega_c+\omega_L)t} \\ E_{Q_x} &\propto J_1(\beta_1)\left[e^{j(\omega_c+\omega_s)t} + e^{j(\omega_c-\omega_s)t}\right] \\ &\quad + jJ_1(\beta_2)\, e^{j(\omega_c+\omega_L)t} \\ E_{Q_y} &\propto J_1(\beta_1)\left[e^{j(\omega_c+\omega_s)t} + e^{j(\omega_c-\omega_s)t}\right] \\ &\quad - jJ_1(\beta_2)\, e^{j(\omega_c+\omega_L)t} \end{aligned} \tag{4}$$

It can be seen that the four output lighwaves all consists of three tones with the same amplitude and frequency configuration, but two tones carrying the signal at $(\omega_c + \omega_s)$ and $(\omega_c - \omega_s)$ have identical phase while the tones bearing the LO at $(\omega_c + \omega_L)$ have 90 deg or 180 deg relative phase differences between them. Then the optical signals are detected by two balanced photodetectors (BPDs) with the output photocurrents,

$$\begin{aligned} i_{BPD1} &= \Re_1\left(E_{I_x}E_{I_x}^* - E_{I_y}E_{I_y}^*\right) \\ &\propto J_1(\beta_1)\, J_1(\beta_2)\left\{\cos\left[(\omega_s-\omega_L)\,t\right]\right. \\ &\quad \left.+\cos\left[(\omega_s+\omega_L)\,t\right]\right\} \end{aligned} \tag{5}$$

$$\begin{aligned} i_{BPD2} &= \Re_2\left(E_{Q_x}E_{Q_x}^* - E_{Q_y}E_{Q_y}^*\right) \\ &\propto J_1(\beta_1)\, J_1(\beta_2)\left\{\sin\left[(\omega_s-\omega_L)\,t\right]\right. \\ &\quad \left.-\sin\left[(\omega_s+\omega_L)\,t\right]\right\} \end{aligned} \tag{6}$$

where $\Re_1$, $\Re_2$ are the responsivities of the two BPDs, respectively. The generated photocurrent from each BPD consists only of two tones at $(\omega_s+\omega_L)$ and $(\omega_s-\omega_L)$ with equal amplitude but inversely relative phase. The two tones in each photocurrents are the copies of the signal but with an up-or down-shifted frequency of ω_L. As the two tones are combined through a 90° electrical hybrid coupler (HC2), the up- and down-converted signals are separated and output from HC2,

$$i_{out-up} \propto J_1(\beta_1)\, J_1(\beta_2)\cos\left[(\omega_s+\omega_L)\,t\right] \tag{7}$$

$$i_{out-down} \propto J_1(\beta_1)\, J_1(\beta_2)\sin\left[(\omega_s-\omega_L)\,t\right] \tag{8}$$

It can be seen that a dual-output microwave photonic frequency up- and down-converter without filtering is realized.

B. High Image Rejection in Down-Conversion

The microwave photonic converter is usually implemented through a heterodyne structure to obtain a nonzero IF signal, therefore, a pair of signals of different frequencies symmetrical about the local oscillator frequency will be generated in transmitter, one of which is a useful signal, and the other is an image interference signal. At the receiving end, when the two signals are input at the same time, the image signal will interfere with the reception of the useful signal, thereby affecting the reception performance. In this paper, the image signal can be suppressed by using the phase cancellation technique. To demonstrate the image rejection capability of our proposed scheme, an input RF/IF signal ω_s along with an additional image signal at ω_{IM} are injected to the MZM simultaneously, as shown by the blue dotted line in Fig. 1. Here we assume the frequency of the RF/IF signal ω_s is higher than that of the LO signal ω_L, so the output of the MZM becomes:

$$E'_{MZM} = E_0 J_0(\beta_1)\, J_1(\beta_1)\begin{bmatrix} e^{j(\omega_c+\omega_s)t} + e^{j(\omega_c-\omega_s)t} \\ +e^{j(\omega_c+\omega_{IM})t} + e^{j(\omega_c-\omega_{IM})t} \end{bmatrix} \tag{9}$$

where $\omega_{IM} = 2\omega_L$-ω_s is the angular frequency of the image signal. Thus, i_{BPD1} and i_{BPD2} becomes:

$$\begin{aligned} i'_{BPD1} &\propto J_0(\beta_1)\, J_1(\beta_1)\, J_1(\beta_2) \\ &\quad \left\{\begin{matrix} \cos\left[(\omega_s-\omega_L)\,t\right] + \cos\left[(\omega_s+\omega_L)\,t\right] \\ +\cos\left[(\omega_L-\omega_{IM})\,t\right] + \cos\left[(\omega_L+\omega_{IM})\,t\right] \end{matrix}\right\} \end{aligned} \tag{10}$$

$$\begin{aligned} i'_{BPD2} &\propto J_0(\beta_1)\, J_1(\beta_1)\, J_1(\beta_2) \\ &\quad \left\{\begin{matrix} \sin\left[(\omega_s-\omega_L)\,t\right] - \sin\left[(\omega_s+\omega_L)\,t\right] \\ -\sin\left[(\omega_L-\omega_{IM})\,t\right] - \sin\left[(\omega_L+\omega_{IM})\,t\right] \end{matrix}\right\} \end{aligned} \tag{11}$$

It can be seen that the image interference signals appear in the two photocurrents with equal amplitude but inversed relative phases. Apply i'_{BPD1} and i'_{BPD2} to a 90° electrical hybrid coupler and the output signal of the down-conversion is given by:

$$i'_{out-down} \propto J_0(\beta_1)\, J_1(\beta_1)\, J_1(\beta_2)\sin\left[(\omega_s-\omega_L)\,t\right] \tag{12}$$

As can be seen from (12), the undesired component $(\omega_L - \omega_{IM})$ and $(\omega_L+\omega_{IM})$ is rejected. By this means, image rejection mixing is successfully realized.

III. Simulation and Result

In order to demonstrate our proposed scheme, a simulation system was built based on Fig. 1. The wavelength of the

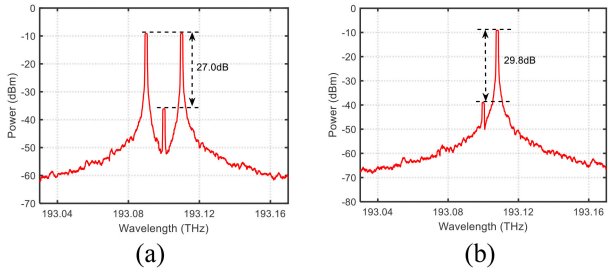

Fig. 2. Optical spectra of the lightwaves from (a) MZM and (b) DPMZM.

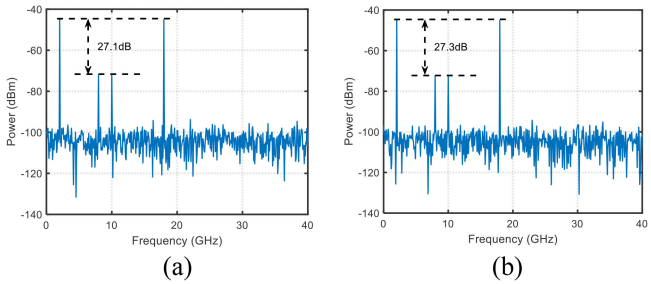

Fig. 3. Electrical spectra of (a) I path and (b) Q path.

lightwave emitted from the LD is 193.1 THz, and the optical power and linewidth are 17 dBm and 10 MHz, respectively. The lightwave is divided into two beams by the optical splitter and injected into the MZM and DPMZM respectively. In the DPMZM, the lightwave is split equally and fed into two parallel sub-MZMs with the half-voltage of 3.5 V.

A. Simultaneous Up- and Down-Conversion Signal Generation

For the simultaneous up- and down-conversion signal generation, a RF/IF signal at 10 GHz is generated by analog signal generator with the power of 19 dBm. The RF/IF signal modulates the lightwave via the MZM working in CS-DSB pattern. At the same time, the LO electrical signal at 8 GHz modulates the lightwave via the DPMZM with an electrical hybrid coupler (HC1) in CS-SSB pattern. The optical spectra of the output signal from MZM and DPMZM are shown in Fig. 2(a) and (b), respectively. It can be seen that both the optical carrier of the RF and LO modulation signals are suppressed, the suppression ratio is about 27.0 dB and 29.8 dB, respectively. In Fig. 2(b), the lower −1st sideband is also suppressed successfully. Since the DPMZM works in small signal modulation mode, the influence of high-order sidebands is negligible. The outputs from the MZM and the DPMZM are injected into 90° optical hybrid and are recombined as four beams with different relative phases. Then they are photodetected by two BPDs with a sensitivity of 1 A/W to generate the I- and Q- path differential photocurrents, and their RF spectra are shown in Fig. 3. It can be seen from the spectra that it contains four tones at 2 GHz, 8 GHz, 10 GHz and 18 GHz, and tones at 2 GHz and 18 GHz are the desired down- and up-converted tones with a dominant magnitudes and orthogonal phases while the tones at 8 GHz and 10 GHz are 27 dB smaller than the main tones, which come from the beating

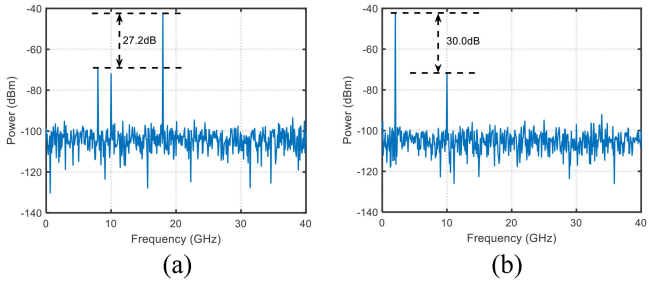

Fig. 4. Electrical spectra of (a) Up-conversion signal and (b) Down-conversion signal.

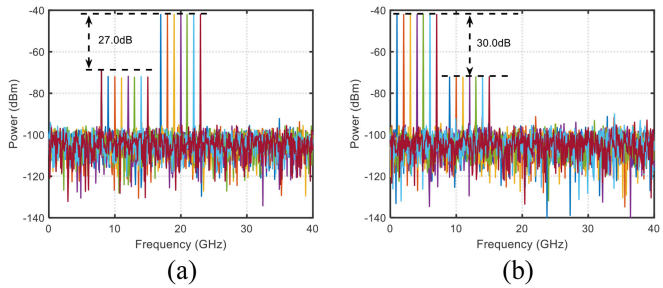

Fig. 5. Measured electrical spectra of the mixed electrical signal for (a) Frequency up-conversion from 17 GHz to 23 GHz and (b) Frequency down-conversion from 1 GHz to 7 GHz. The LO signal is 8 GHz.

between the residual optical carrier and the LO and RF signal modulated optical sidebands. Then the electrical signals from the two BPDs are injected into 90° electrical hybrid coupler (HC2) to separate the two main tones based on their phase orthogonality, and the electrical spectra of the two output ports are given in Fig. 4. It can be seen from Fig. 4(a) that the down-converted signal at 2 GHz is cancelled out completely and the up-converted signal at 18 GHz is dominant and the unwanted signal suppression ratio is 27.2 dB. Since the unwanted tone at 8 GHz is also cancelled out, the down-converted signal at 2 GHz, as shown in Fig. 4(b), suffer only a little smaller distortion from the spur at 10 GHz with the unwanted signal suppression ratio of 30.0 dB. Therefore, a dual-output microwave photonic frequency up- and down-converter without filtering is successfully achieved.

To demonstrate the wide tunability of up- and down-converter, we tuned the RF signal from 9 GHz to 15 GHz by a step of 1 GHz. With a fixed 8 GHz LO signal, an up-conversion range of 17–23 GHz and a down-conversion range of 1–7 GHz is respectively achieved, as shown in Fig. 5(a) and (b). It can be seen that the mixing spurs are suppressed by 27.0 dB and 30.0 dB, respectively. The tuning range of the converter is related to the LO frequency and the bandwidth of the 90° electrical hybrid coupler.

In order to verify the quality of the output signal of the converter, we analyze the conversion gain and noise figure (NF) of the system. The RF/IF frequency and the LO frequency are set to 10 GHz and 8 GHz, respectively. The RF/IF power is set to 10 dBm. The LO power levels are tuned from 5 dBm to 20 dBm. The conversion gain and NF are shown in the Fig. 6(a) and (b). It can be seen that the conversion gain increases with the increase of LO power, showing a linear relationship. The noise

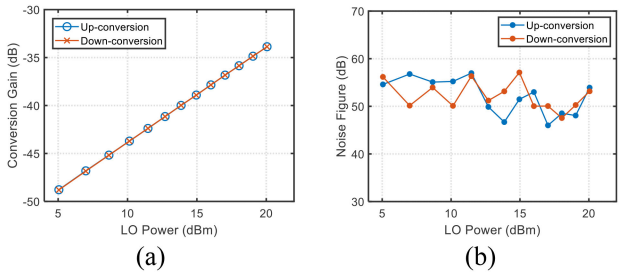

Fig. 6. Measured (a) Conversion gain and (b) NF for different LO power of the system.

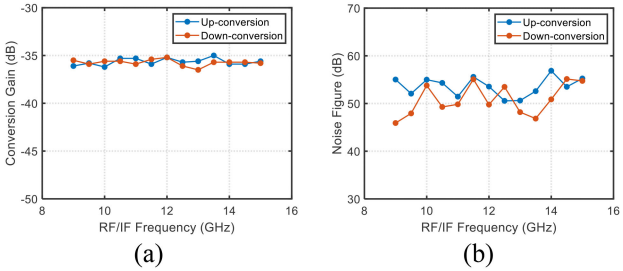

Fig. 7. Measured (a) Conversion gain and (b) NF for different RF/IF frequency of the system.

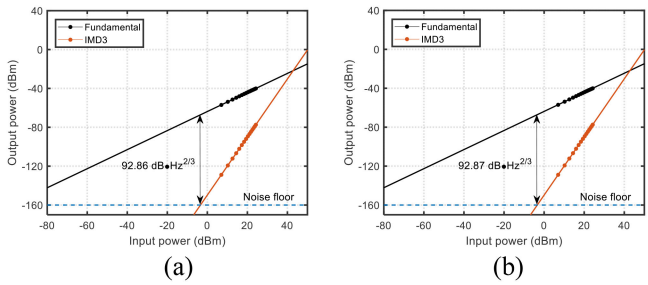

Fig. 8. Dynamic range performance of (a) Up-conversion and (b) Down-conversion.

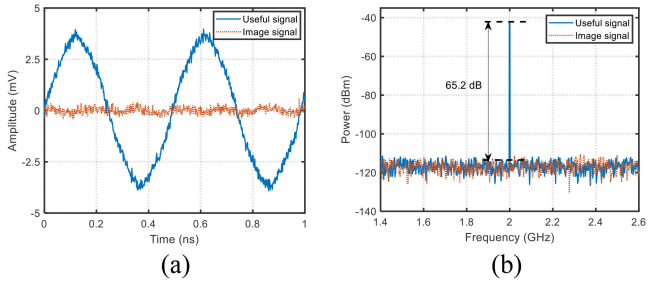

Fig. 9. Measured (a) Waveforms and (b) Spectra of the down-conversion IF signal (blue solid line) and image IF (orange dotted line) signal from the IRM.

figure shows a fluctuating trend with the increase of LO power, with an average of 52 dB.

Then, the conversion gain and NF for different RF/IF frequency is measured. The LO power is set to 19 dBm. When the RF/IF frequency is tuned from 9 to 15 GHz at a step of 0.5 GHz, and the LO frequency is adjusted correspondingly from 7 to 13 GHz to make the IF frequency be fixed at 2 GHz in down-conversion, or from 9 to 3 GHz to make the output frequency be fixed at 18 GHz in up-conversion. The conversion gain and NF for different RF/IF frequency are shown in Fig. 7(a) and (b). As can be seen, the conversion gain is around -35.7 dB with a fluctuation of about 0.5 dB in the frequency range from 9 to 15 GHz. The noise figure shows a fluctuating trend with the increase of RF frequency, with an average of 53 dB in up-conversion and 51 dB in down-conversion. In this scheme, the laser and BPDs generate noise, which affects the system. Noise figure can be effectively optimized by using lower noise laser and BPDs. In order to improve the conversion gain, EDFA can be added to the system, but EDFA will introduce noise, which will degrade the noise figure. In actual use, the conversion gain and noise figure should be considered together to optimize the system performance as well as possible.

Due to the nonlinear effects of the modulator, some undesired frequency components also appear around the useful IF components with angular frequencies of $(\omega_s + \omega_L)$ and $(\omega_s - \omega_L)$. Among these unwanted frequency components, the third-order intermodulation (IMD3) near the IF frequency can hardly be filtered out by an electrical filter. Therefore, the IMD3 is considered to be the most important factor limiting the dynamic range of microwave mixers. To check the impact of IMD3, we measured the spurs free dynamic range (SFDR) to test the dynamic range of this system. A two-tone RF signals of 10 GHz and 10.1 GHz were applied to the converter. As shown in Fig. 8, the SFDR of the frequency up-conversion and down-conversion are 92.86 dB·Hz$^{2/3}$and 92.87 dB·Hz$^{2/3}$, respectively. The noise floor is assumed as -160 dBm/Hz.

B. High Image Rejection in Down-Conversion

To verify the image rejection performance in down-conversion, we change the frequency of the RF signal into the frequency of the image signal (i.e., 6 GHz) [12]. The waveform and spectrum of the image IF signal are shown as the dotted lines in Figs. 9(a) and 9(b), and the waveform and electrical spectrum of the useful IF signal are shown as the solid lines. As can be seen from Fig. 9(a), the amplitude of image signal is just about zero. Fig. 9(b) shows that the image IF signal at 2 GHz is successfully suppressed. These mean an IRM with an IRR of 65.2 dB is realized and it is better than most of the commercially accessible electrical IRMs (typically $\sim$30 dB).

Since the real integrated 90° optical hybrid usually has a certain phase drift, it will degrade the phase cancellation performance. Therefore, it is necessary to analyze how much the phase drift affects the image rejection function. According to the performance parameters of the integrated 90° optical hybrid device, we simulate the situation when the phases of I path and Q path are imbalanced in the range of 85$\sim$95 deg, as shown in Fig. 10.

When the phase starts to deviate from 90°, the IRR drops rapidly, which means that the image rejection performance is greatly affected by the phase deviation. In fact, limited by the current manufacturing technology, commercial 90° optical hybrid usually have a phase deviation within $\pm$5 deg, and it is difficult to compensate by other methods, which leads to the

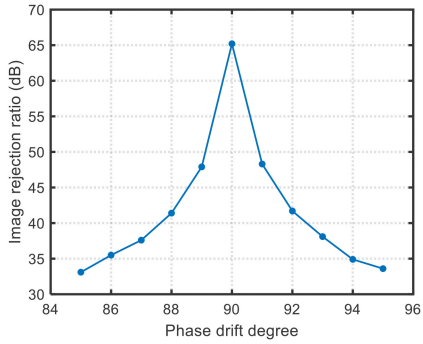

Fig. 10. Measured image rejection ratio when the 90° optical hybrid has a phase drift from 85° to 95°.

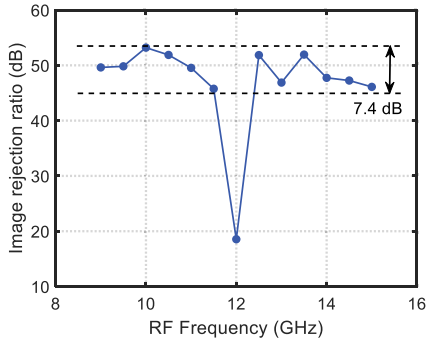

Fig. 11. Measured image rejection ratio when RF signal frequency changes from 9 GHz to 15 GHz. The LO signal is fixed at 8 GHz.

occurrence of phase inaccuracy [19]. As shown in Fig. 10, when the phase difference drifts to ±5 deg, the IRR is still above 33 dB, comparable with the IRR of the traditional electrical image-reject mixer (about 30 dB) [20].

In order to further verify the stability of the image rejection function, we change the frequency, amplitude and phase of the input RF signal to test the variation of the image rejection ratio. When the phase difference between the I path and the Q path is exactly 90°, the interference of the image signal is completely suppressed. In a perfectly ideal situation, as the input signal amplitude increases, the image rejection ratio increases. Unfortunately, this is unlikely to happen in practice. Therefore, in order to make the analysis results more in line with the actual situation, we adjust the phase difference between the I path and the Q path to 89° (introducing a 1° phase drift). The results obtained are shown in Figs. 11 and 12.

As can be seen from Fig. 11, when the receiving IF signal and image signal have different frequency, the image rejection ratio can remain relatively large value about 50 dB; while, as they have equal frequency, the image rejection ratio drops sharply to less than 20 dB. This attributes to the fact that the limited extinction ratio of the MZM of 45 dB in our simulation leads to the incomplete suppression of the optical carrier. To solve this problem, an optical modulator with a larger extinction ratio is prefer.

In order to explore the influence of the input signal amplitude and phase on the image rejection ratio, we adjust the relevant parameters. The results are shown in Fig. 12(a) and (b).

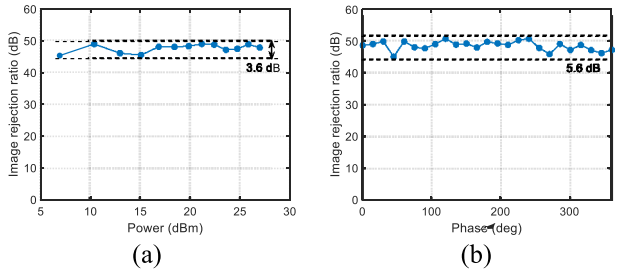

Fig. 12. Measured image rejection ratio when RF signal (a) Power changes from 7 dBm to 27 dBm and (b) Input phase changes from 0° to 360°. RF and LO signal frequency are fixed at 10 GHz and 8 GHz, respectively.

TABLE I
THE FACTORS THAT AFFECT THE IMAGE REJECTION RATIO

Factor	IRR Maximum Difference (dB)	Degree of Influence on IRR	Can Be Compensated
Phase drift	31.8	Severe	No
Frequency variation	7.4*	Mild	Yes
Amplitude variation	3.6	Mild	N/A
Phase variation	5.6	Mild	N/A
Half-voltage imbalance	41.5	Severe	Yes

* When the RF frequency is not 12 GHz, the maximum difference in IRR is 7.4 dB.

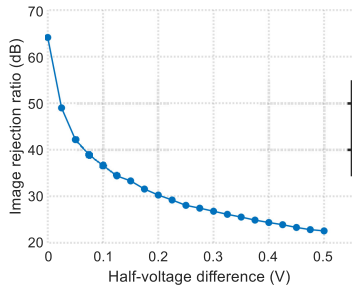

Fig. 13. Measured image rejection ratio when the half-voltage of the two sub-MZMs is different.

We can see that the image rejection ratios are all above 40 dB, and the input signal amplitude and phase have little effect on the image rejection ratio. The difference between the maximum and minimum values is 3.6 dB and 5.6 dB, respectively.

It is assumed in this paper that the two sub-MZMs of the DPMZM have equal half-voltage. However, in actual situations, due to the influence of external factors such as manufacturing process and operating temperature, the half-voltage of the two sub-MZMs may not be equal. In response to this problem, we have simulated and analyzed the situation when the half-voltage of the sub-MZMs is not equal, as shown in Fig. 13.

TABLE II
COMPARISON BETWEEN MICROWAVE PHOTONIC FREQUENCY CONVERTERS

Ref.	Structure	Functions	Gain (dB)	NF (dB)	SFDR (dB·Hz$^{2/3}$)	IRR (dB)
[14]	DPol-DPMZM, 90° OH	Up- and down-conversion, IRM	N/A	N/A	114	32.3
[15]	MZM+DPol-MZM, 90° OH	Down-conversion, IRM	N/A	N/A	N/A	> 53
[16]	PolM+MZM, 90° OH	Multi-band transmitter and receiver	N/A	N/A	101	30
[17]	DP-DMZM	Up- and down-conversion	-26	N/A	108.3	N/A
[18]	AOM+MZM, 90° OH	Dual band up conversion	N/A	N/A	122.1	N/A
This work	DPMZM+MZM,90° OH	Up- and down-conversion, IRM	-35.7	52	92.8	65.2

NF: noise figure; SFDR: spurs free dynamic range; IRR: image rejection ratio; IRM: image reject mixer; OH: optical hybrid

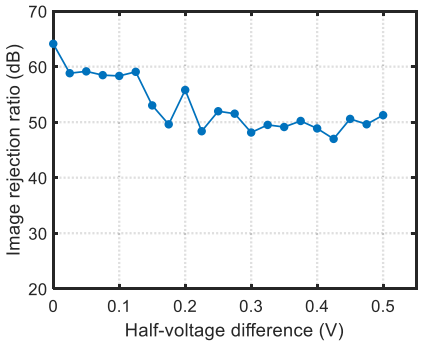

Fig. 14. Measured image rejection ratio after compensation when the half-voltage of the two sub-MZMs is different.

It can be seen that when the half-voltage of the two sub-MZMs differ by 0.025 V, the image rejection ratio is seriously reduced to 48.9 dB. As the half-voltage difference continues to increase, the image rejection ratio decreases slowly. When the half-voltage differs by 0.5 V, the image rejection ratio drops to 22.5 dB. Since the image rejection ratio of commercial electrical IRMs can generally reach 30 dB, we can tolerate a half-voltage imbalance of 0.2 V.

Since the half-voltage imbalance will reduce the suppression of the optical carrier and sidebands, thus affecting the image rejection ratio. To compensate for this imbalance, we control the bias voltage injected into the two sub-MZMs so that the two sub-MZMs always operate at the minimum transmission point. The compensation result of the half-voltage imbalance is shown in Fig. 14. At the same time, we add an electrical attenuator to control the power of the electrical signal driving the two sub-MZMs, thereby optimizing the effect of CS-SSB modulation. It can be seen from the figure that the image rejection ratio after compensation is kept above 45 dB, indicating that our image rejection compensation scheme is feasible.

The factors that affect the image rejection ratio are shown in Table I. The main factors affecting the image rejection ratio are phase drift of the 90° optical hybrid and half-voltage imbalance of the DPMZM sub-modulators. Half-voltage imbalance can be compensated by adjusting DC bias voltage and RF signal input power, but phase drift cannot be accurately compensated, so phase drift is the dominant factor affecting image rejection performance.

IV. COMPARISON AND DISCUSSION

To compare our scheme with the reported works in the literatures, structural characteristics and performances of different kinds of microwave photonic converters are listed in Table II. In [14]–[16], polarization modulators (DPol-DPMZM, DPol-MZM, PolM) are used for signal modulation, which impose strict requirements on the orthogonality of x-polarization and y-polarization. In actual cases, the deviation of the polarization orthogonality will degrade the image rejection ratio. Compared with [14]–[16], our scheme uses DPMZM and MZM, which can avoid the influence of polarization on the image rejection ratio and leads to a higher image rejection ratio. In [17], the up-conversion signal and the down-conversion signal cannot be generated at the same time, and by adjusting the dc bias voltage of the modulator to achieve either up- or down-conversion switching, which brings inconvenience to practical use in some applications. Moreover, because of its single-ended output structure, image rejection is not possible with this structure. Our scheme adopts the I/Q output structure, which can realize the simultaneous generation of up- and down-converted signals and the image rejection function through the phase cancellation technique. In [18], AOM and MZM are used to realize dual-band up-conversion function. Due to the narrow modulation bandwidth and low center frequency of AOM, it can only be applied to up-conversion, but cannot well realize the down-conversion function of wide-range tuning in 8–12 GHz band. In our scheme, DPMZM is used instead of AOM, and has a large tunable range, which means more application scenarios.

V. CONCLUSION

This paper has proposed a dual-output microwave photonic frequency up- and down-converter without filtering based on

a 90° optical hybrid. By using DPMZM and MZM to realize CS-SSB and CS-DSB modulation, the optical carrier and the lower −1st sideband of the LO signal have successfully been suppressed without using any wavelength-dependent filter. Up and down converted signals can be generated simultaneously and output separately through a 90° optical hybrid and a 90° electrical hybrid coupler. Simulation results show that the 10 GHz RF/IF signal is up (down)-converted to 18 (2) GHz by an 8 GHz LO signal. The unwanted signal suppression ratio is 27.2 dB and 30.0 dB, respectively. With a fixed 8 GHz LO signal, an up-conversion range of 17–23 GHz and a down-conversion range of 1–7 GHz are achieved respectively. By adjusting the frequency of the LO signal, flexible adjustment of different frequency ranges can be realized. In addition, we have tested and analyzed the conversion gain, noise figure and SFDR of the system. For high image rejection mixing in down-conversion, the IRR is about 65.2 dB, and the effects of phase drift, frequency, amplitude and phase variation on the image rejection function are analyzed. Finally, the influence of half-voltage imbalance of the DPMZM sub-modulators on the image rejection function is analyzed, and a compensation method is given. Due to the wide operating bandwidth and flexibility of the proposed converter, it can find lots of applications in radar transceiver, satellite repeater, electronic warfare and broadband wireless communication systems.

REFERENCES

[1] Z. Tang, Y. Li, J. Yao, and S. Pan, "Photonics-based microwave frequency mixing: Methodology and applications," *Laser Photon. Rev.*, vol. 14, no. 1, Jan. 2020, Art. no. 1800350.

[2] C. Huang and E. H. W. Chan, "Photonics-based single sideband mixer with ultra-high carrier and sideband suppression," *IEEE Photon. J.,* vol. 13, no. 4, Aug. 2021, Art no. 7200308.

[3] S. Pan *et al.*, "Satellite payloads pay off," *IEEE Microw. Mag.*, vol. 16, no. 8, pp. 61–73, Sep. 2015.

[4] Y. Gao and S. Gao, "Premodulation-free microwave frequency up/down-conversion using optical-fiber-stimulated Brillouin scattering," *J. Nonlinear Opt. Phys. Mater.*, vol. 18, no. 4, pp. 701–707, Dec. 2009.

[5] Y. Wang, W. Zhou, Y. Ding, T. Meng, W. Dong, and X. Zhang, "Simple and flexible all-optical microwave photonic frequency converter based on stimulated Brillouin scattering effect," *IEEE Photon. J.,* vol. 12, no. 5, Oct. 2020, Art no. 7801108.

[6] Z. Tang, F. Zhang, D. Zhu, X. Zou, and S. Pan, "A photonic frequency downconverter based on a single dual-drive Mach-Zehnder modulator," in *Proc. IEEE Int. Topical Meeting Microw. Photon.*, 2013, pp. 150–153.

[7] Y. Gao *et al.*, "An efficient photonic mixer with frequency doubling based on a dual-parallel MZM," *Opt. Commun.,* vol. 321, pp. 11–15, 2014.

[8] Z. Tang and S. Pan, "Image-reject mixer with large suppression of mixing spurs based on a photonic microwave phase shifter," *J. Lightw. Technol.*, vol. 34, no. 20, pp. 4729–4735, Oct. 2016.

[9] Y. Gao, A. Wen, W. Jiang, Y. Fan, and Y. He, "All-optical and broadband microwave fundamental/sub-harmonic I/Q down-converters," *Opt. Exp.*, vol. 26, no. 6, pp. 7336–7350, Mar. 2018.

[10] D. Zhu and S. Pan, "Photonics-based microwave image-reject mixer," *Photonics*, vol. 5, no. 2, Jun. 2018, Art. no. 6.

[11] Z. Tang and S. Pan, "A reconfigurable photonic microwave mixer using a 90° optical hybrid," *IEEE Trans. Microw. Theory Techn.*, vol. 64, no. 9, pp. 3017–3025, Sep. 2016.

[12] Z. Tang and S. Pan, "Reconfigurable microwave photonic mixer with minimized path separation and large suppression of mixing spurs," *Opt. Lett.*, vol. 42, no. 1, pp. 33–36, Jan. 2017.

[13] J. Li *et al.*, "Full-band direct-conversion receiver with enhanced port isolation and I/Q phase balance using microwave photonic I/Q mixer," *Chin. Opt. Lett.*, vol. 15, no. 1, Jan. 2017, Art. no. 010014.

[14] Z. Shi, S. Zhu, M. Li, N. Zhu, and W. Li, "Reconfigurable microwave photonic mixer based on dual-polarization dual-parallel Mach-Zehnder modulator," *Opt. Commun.*, vol. 428, pp. 131–135, Dec. 2018.

[15] D. Zhu, X. Hu, W. Chen, D. Ben, and S. Pan, "Photonics-enabled simultaneous self -interference cancellation and image-reject mixing," *Opt. Lett.*, vol. 44, no. 22, pp. 5541–5544, Nov. 2019.

[16] W. Chen, D. Zhu, J. Liu, and S. Pan, "Multi-band RF transceiver based on the polarization multiplexed photonic LOs and mixers," *IEEE J. Sel. Topics Quantum Electron.*, vol. 27, no. 2, Mar./Apr. 2021, Art no. 7601009.

[17] Q. Guo, E. Xu, and Z. Zhang, "Switchable and filter-free photonic microwave single-sideband frequency converter," *Microw. Opt. Technol. Lett.*, vol. 63, no. 4, pp. 1073–1077, 2021.

[18] J. Ding, D. Zhu, B. Zhang, and S. Pan, "Dual-output filter-free microwave photonic single sideband up-converter with high mixing spur suppression," *Appl. Opt.*, vol. 60, no. 26, pp. 7888–7893, Sep. 2021.

[19] H. Li *et al.*, "A filterless reconfigurable frequency mixer based on a wideband photonic microwave phase shifter," *Opt. Commun.*, vol. 475, Nov. 2020, Art. no. 126224.

[20] T. Zhang, J. Du, and Y. J. Guo, "An 8–10-GHz low-loss image-reject HTS mixer based on cascaded Josephson junctions," *IEEE Microw. Wireless Compon. Lett.*, vol. 31, no. 8, pp. 945–948, Aug. 2021.